Neutron irradiated perovskite films and solar cells on PET substrates

Neutron irradiated perovskite films and cells on PET substrates

F. De Rossi[1,], B. Taheri[1], M. Bonomo[2,*], V. Gupta[3], G. Renno[2], N.Yaghoobi. Nia[1], P. Rech[4], C. Frost[5], C. Cazzaniga[5], P. Quagliotto[2], A. Di Carlo[1,6], C. Barolo[2,7], M. Ottavi[3,*], F. Brunetti[1,*]*

[1] *CHOSE, Department of Electronic Engineering, University of Rome Tor Vergata, via del Politecnico 1, 00133 Rome, Italy*

[2]*Department of Chemistry, NIS Interdepartmental Centre and INSTM Reference Centre, Università degli Studi di Torino, Via G. Quarello 15A, 10135 – Turin, Italy*

[3] *Department of Electronic Engineering, University of Rome Tor Vergata, via del Politecnico 1, 00133 Rome, Italy*

[4]*Universidade Federal do Rio Grande do Sul (UFRGS), Brazil*

[5]*ISIS facility, UKRI-STFC, , Rutherford Appleton Laboratory, Didcot, OX11 0QX, United Kingdom*

[6] *CNR-ISM Istituto di Struttura della Materia, via del Fosso del Cavaliere 100, 00133 Rome, Italy*

[7]*ICxT Interdepartmental Centre, Università degli Studi di Torino, Via Lungo Dora Siena 100, 10153 – Turin, Italy*

**co-corresponding authors: francesca.de.rossi@uniroma2.it; matteo.bonomo@unito.it; ottavi@ing.uniroma2.it; francesca.brunetti@uniroma2.it*

Abstract

Flexible perovskite solar cells feature high power-per-weight ratio and low cost manufacturing, which make them very attractive for space and avionic applications. It is thus paramount to assess their response to the harsh space environment. Although an increasing number of studies have been investigating the effect of electron and proton radiation on perovskite solar cells, very few have dealt with neutron irradiation and even less with flexible devices. In this paper, the stability of flexible perovskite solar cells against fast neutron irradiation is evaluated, comparing commercially available spiro-OMeTAD and an in-house modified P3HT as the hole transport materials. We observed that modified-P3HT cells experienced smaller voltage and current losses compared to spiro-OMeTAD but the overall performance suffered a much higher drop, as a consequence of a larger decrease in fill factor, ascribable to a sub-optimal perovskite/polymer interface. Nonetheless, spectral

response and behavior at different light intensities of modified-P3HT cells suggest the polymer to be potentially more resilient than spiro-OMeTAD under fast neutron irradiation, once the perovskite/polymer will be improved.

Keywords

Flexible perovskite solar cells; neutron irradiation; space; hole transport material; small molecule; P3HT.

1. Introduction

High efficiency, low cost and processability from solutions are key advantages of perovskite-based devices over conventional silicon-based photovoltaics, and have attracted soaring attention from both academia and industry[1–4]. While long-term stability of these devices is still an open issue, the increasing understanding of materials and degradation mechanisms is leading to promising improvements in both accelerated indoor and outdoor tests[5–9].

When moving from rigid glass to flexible plastic substrates, power conversion efficiency (PCE) drops from over 25%[10] to 19.5%[11]; nonetheless, flexible perovskite solar cells (f-PSC)[12,13] allow for low temperature and low cost manufacturing processes[14–16], open up to a wider range of applications[17,18] and are more sustainable[19]. Moreover, thanks to substrate conformability and superior power-to-weight ratio[20], f-PSCs show enormous potential for avionic and space applications, where the payload is a major concern[21]. Interestingly, some of the extrinsic factors affecting PSC long-term stability, such as humidity and oxygen, which can potentially undermine their applicability on earth[7], do not apply in space[21]. On the other hand, space is a harsh environment[22], featuring large radiation doses of highly energetic particles, such as electrons, protons, and heavy ions , i.e. cosmic rays, and extreme temperature cycles, whose effect on PSC performance and stability need to be assessed.

A rising number of studies, carried out to investigate the effect of outer space radiations on PSCs, has reported good tolerance to both electrons and protons. Glass-encapsulated cells

with glass/FTO/TiO_2/perovskite/P3HT/Au structure survived fluence levels of up to 10^{16} and 10^{15} particles·cm^{-2} of electrons (1 MeV) and protons (50 keV) respectively, levels known to completely destroy c-Si, GaAs and InGaP/GaAs in spacecrafts[22]. Cells on quartz substrates, with AZO/SnO_2/CsMAFAPbIBr/spiro-OMeTAD/Au structure, did not show significant loss in efficiency when exposed to up to 10^{13} particles·cm^{-2} of protons (150 keV)[21]. Devices on glass, with ITO/PEDOT:PSS/MAPI/PCBM/BCP/Ag layer sequence, withstood fluences of up to 10^{13} particles·cm^{-2} of high-energy (68 MeV) protons [23,24], outperforming c-Si devices; the same cell structure on PET (the only report on flexible substrates so far) also demonstrated to be stable against fluences of up to 10^{12} particles·cm^{-2} of low-energy (100 keV) protons, expected to be stopped in the shallower regions of the devices, and thus to lead to degradation more likely than high-energy protons[25]. Such remarkable resilience to both electrons and protons has been ascribed to the self-healing properties of the mixed covalent-ionic lattice of the perovskite materials, which allows self-passivation of the radiation-induced defects[23].

Less attention has been dedicated to assessing the interaction between neutrons and PSCs, even though fast neutrons (i.e. with energies > 10 MeV) represent one of the most severe forms of radiation at aircraft altitudes, in avionic, and space environments. For example, the annual fluence received by the equipment on the International Space Station (ISS) is estimated to be ~2.8×10^{11} neutrons·cm^{-2} with energies from 0.1 eV to 10^5 MeV[26]. As a reference, at ground level the fluence is 3.85×10^5 neutrons·cm^{-2}[26]. Fast neutrons are known to be a threat for microelectronic components in both space and terrestrial environment, as they can induce transient faults, such as bit-flips, or permanent degradation, such as displacement damage (one or more atoms are removed from their original locations by the impinging particle) caused by the accumulation of charge, i.e. total ionizing dose[25,27].

A recent preliminary work evaluated the resilience of planar PSCs, with inverted p-i-n structure on glass substrates, to thermal and fast neutrons, using the VESUVIO beamline at the ISIS Spallation Neutron Source[28]. Glass-encapsulated devices, with cell structure ITO/ PEDOT:PSS/ CH3NH3Pb$I_{3-x}Cl_x$/ PCBM/ aluminium, showed good stability to 435 minutes of neutron irradiation, i.e. 1.5×10^9 neutrons·cm^{-2}, corresponding to approximately 80 years of

fast neutron exposure on the ISS. Fast neutrons led to irreversible effects, possibly due to atomic displacement in the active materials, albeit mitigated by the formation of neutron-induced shallow traps, acting as dopants[28].

In this paper, we report on unencapsulated flexible PSCs, potentially better fit to avionic and space applications than glass-based ones, upon fast neutron irradiation at fluence levels of, respectively, 1.39×10^9 neutrons·cm^{-2} (same order of magnitude as in ref[28], i.e. almost 80 years of fast neutron exposure on the ISS) and 1.62×10^{10} neutrons·cm^{-2} (equivalent to 864 years of fast neutron exposure on the ISS).

Both spiro-OMeTAD, and a benzothiadiazole-modified P3HT (BTD-P3HT)[29] were used and compared as the hole transport material (HTM). Spiro-OMeTAD is possibly the most widely used HTM for PSC in research laboratories: although stability issues have been reported, related to additives used to dope it and increase its conductivity[30,31], record PSC devices usually employ spiro-OMeTAD as the HTM[32,33]. P3HT polymers have been reported to be an effective alternative to costly spiro-OMeTAD, thanks to high hole mobility (0.1 cm^2 V^{-1} s^{-1}), relatively easy synthesis, thus lower production costs, and good thermal and light stability [34–37], and have been successfully used for planar n-i-p PSC on flexible substrates, achieving a power conversion efficiency (PCE) of 11.84%[38]. Furthermore, this work's choice of using BTD-modified P3HT instead of conventional P3HT rely on previous encouraging results: PCE comparable to P3HT, feasibility for large area deposition leading to 6.9% PCE on a 6x6 cm^2 module, improved stability under illumination compared to both unmodified P3HT and spiro-OMeTAD[29].

2. Results and discussion

Planar perovskite solar cells with n-i-p structure, i.e. SnO_2/ perovskite/ hole transport layer/ Au, were fabricated on flexible ITO-PET via spin-coating of tin oxide (SnO_2), mixed-cation mixed-halide perovskite $Cs_{0.06}FA_{0.78}MA_{0.16}Pb(I_{0.84}Br_{0.16})_3$ and either commercially available spiro-OMeTAD or in-house synthesised BTD-P3HT[29], topped with a thermally evaporated gold electrode. Both spiro-OMeTAD and BTD-P3HT were doped with the same additives, i.e.

tert-butyl pyridine, Li-TFSI and Co(III)-TFSI, but at different concentrations, according to our previous work[36].

Figure 1 shows the PV parameters, extracted by the current density-voltage (J-V) curves, of the flexible solar cells, tested after fabrication. Spiro-OMeTAD cells display higher PCE than BTD-P3HT: 12% vs 9.2% in average for the reverse scan, 10.9% vs 8.5% in average for the forward scan, 14.3% vs 10.8% for the best device. Open circuit voltages (V_{OC}) range between 1009 mV and 1038 mV for spiro-OMeTAD and between 944 mV and 1009 mV for BTD-P3HT (Figure S 1). The lower values for the polymer are possibly due to additional non-radiative recombination at the interface with perovskite: strong electronic coupling and poor physical contact between highly regioregular, flat BTD-P3HT and perovskite can slow the hole transport[39], whereas spiro-OMeTAD small molecules arrange more effectively on the perovskite, leading to a higher quality interface and promoting hole transport. The lower short circuit current density (J_{SC}), ranging between 17.5 and 19.3 mA/cm^2 for spiro-OMeTAD and between 15.6 and 17.6 mA/cm^2 for BTD-P3HT, and fill factors (FF), 67% and 58% in average for spiro-OMeTAD and BTD-P3HT respectively (Figure S 1) can be related to the short chain of the polymer[40], whose molecular weight is 44.9 kDa[29]. Also, the less favourable band alignment for BTD-P3HT, whose highest occupied molecular orbital (HOMO) lies at -5.14 eV[29] whilst it is -5.23 eV for spiro-OMeTAD, can lead to transport barriers and internal voltage drop, particularly around the maximum power point, contributing to the low FF[41].

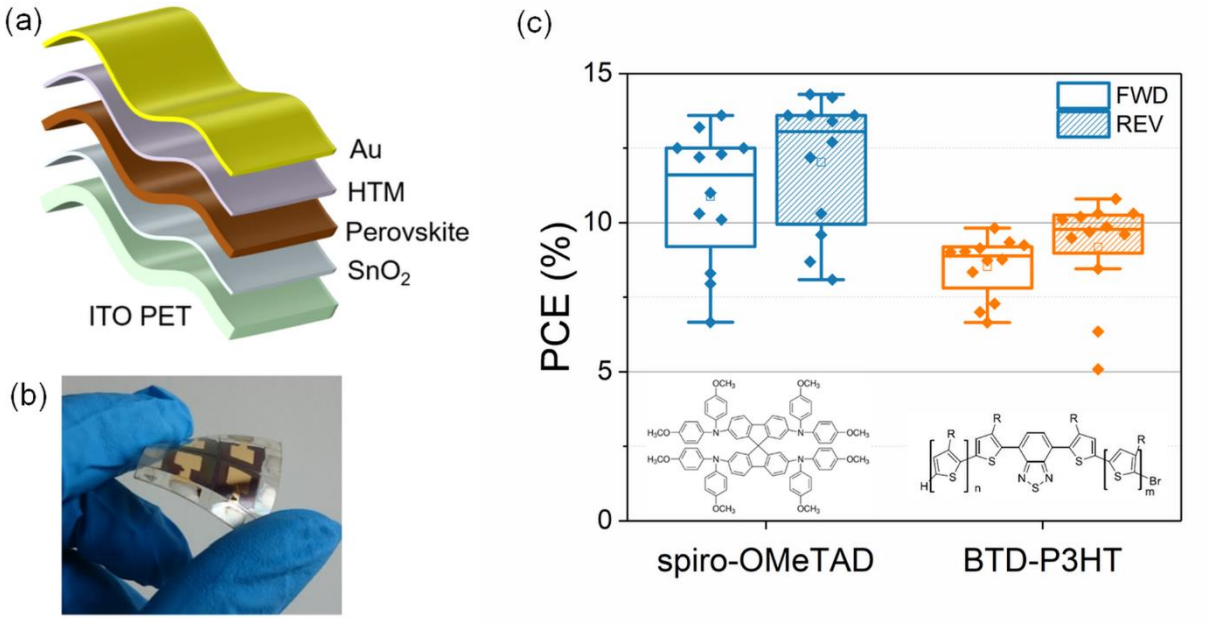

Figure 1. ***Flexible cells used in this study****. (a) Scheme of the cell architecture; (b) Picture of a typical flexible device, including 4 squared cells on the same substrate, electrically isolated by laser scribing; (c) power conversion efficiency of freshly fabricated flexible cells, endowed with either commercially available spiro-OMeTAD or in-house synthesised BTD-P3HT (R = hexyl group).*

After characterisation, cells destined to be exposed to the accelerated neutron beam were carefully packaged without exposing them to light and shipped over to the ChipIR facility at the ISIS Spallation Neutron Source of the Rutherford Appleton Laboratory in Didcot (United Kingdom).

ChipIR beamline provides a high energy neutron spectrum of energy that resembles the atmospheric one, although accelerated (Figure S 2), and is mainly used for the analysis of single event effects (SEEs) in electronic component at ground and flight level [42].The neutron flux available at ChipIR is about 2.5×10^6 neutrons·cm^{-2}·s^{-1}, almost 8 orders of magnitude higher than the atmospheric neutron flux at sea level, i.e. 3.6×10^3 neutrons·cm^{-2}·h^{-1}, allowing to gather a statistically significant amount of neutrons interactions in a very short time. ChipIR neutrons interactions resemble also the radiation environment of other planets, such as Mars, and of the interior of space crafts, such as the International Space Station, where neutrons spectra are similar to the terrestrial one (Figure S 2). This is because in all these environments the production of neutrons is based on the spallation reaction of high energy primary protons. This would not be the case, for example, at a fission reactor,

where the neutron energy spectrum does not extend to the high energies (say E >10 MeV) . Unlike other beamlines, such as VESUVIO, ChipIR provides a neutron flux nearly free from thermal neutrons (i.e. low energy neutrons produced by the interaction of high energy neutrons with materials) and allows focusing on high energy neutrons (fast neutrons), which are strongly correlated to high energy protons, reportedly affecting electronic devices [43]. Also, the high energy neutron flux of ChipIR is about 100 times the one on VESUVIO, allowing to deliver the same fluence in a much shorter time.

Unencapsulated flexible cells were exposed to fluences of about 10^9 neutrons·cm^{-2} and 10^{10} neutrons·cm^{-2} to highlight eventual incremental effects. ITO-PET substrates, bare and coated with SnO_2, were also irradiated: only slight differences in the transmittance were observed (Figure S 3), confirming the resilience of both the plastic substrate, where ITO acts as a protection layer[44], and the electron transport layer [21]. On the contrary, perovskite layers, deposited on SnO_2, heavily suffered from irradiation, as proved in the XRD spectra (Figure S 4) by the prominence of the peak ascribable to PbI_2 (003), located at 2θ = 12.6°, over the one characteristic of the PSK (100) film, located at 2θ = 14.1°. Nevertheless, the analysis on perovskite/HTM layers revealed the protective behaviour of HTM against perovskite degradation: the ratio between the integrated areas of this two peaks is close to 8 for the perovskite film but it is much lower, i.e. $\approx$ 4, when a HTM-protected PSK layer is irradiated, accounting for sizeable shielding effect of the HTM. The analyses were limited to the film of the most performing devices, based on spiro-OMeTAD, and to the worst scenario, 10^{10} neutrons·cm^{-2}.

Due to the lack of a solar simulator at the ISIS facility, the f-PSC performance could not be measured immediately before and after irradiation. It took 21 days before the irradiated cells could be retested, due to the shipping time and the post-irradiation quarantine required for safe handling, according to ISIS safety protocols. During this time, the control cells were kept in the fabrication laboratory, stored in a box with silica in the dark at ambient conditions.

The effect of the storage time on control devices was assessed to disregard any contributions to degradation, ascribable to the mere ageing process: J-V characteristics of

control f-PSCs were measured after 21 days and compared to those recorded right after fabrication.

As shown in Figure 2 (a), the performance of the control spiro-OMeTAD cells worsened overall, from average PCE of 12.2% and 10.9% (reverse and forward scans) to 9.8% and 9.2%. The J-V curves reported in Figure 2 (c), which represent an average of four devices, show a reduction of current density and FF as well as an increase of the series resistances. Also the standard deviation associated to the average J-V curve increased from 9% for the fresh devices to 17% for the cells after the storage in dark, in line with the increased spread of the PV values shown in Figure S 5. The observed degradation can be ascribed to the presence of the additives, broadly used to enhance spiro-OMeTAD conductivity, which are known to degrade when exposed to oxygen and humidity [45,46]. The same additives that induce degradation in spiro-OMeTAD have been found to improve the stability of P3HT[36], that has already been reported to be more stable, thanks to its low permeability to oxygen and strong hydrophobicity[34,47]. The polymer likely shields the dopants better than spiro-OMeTAD from getting in contact with humidity and air. Actually, control BTD-P3HT cells did not suffer from the storage time, passing from 9.6% and 9.3% average PCE (reverse and forward scans) for pristine cells, to 10.4% and 9.1% average PCE after storage. Only the hysteresis slightly increased, as also evident from the average J-V curves in Figure 2 (d), due to an improvement in the reverse scan and a worsening in the forward scan. Unlike the spiro-OMeTAD case, the standard deviation of the average J-V curves went from 6% for the fresh cells to 7% for the devices after the storage in dark.

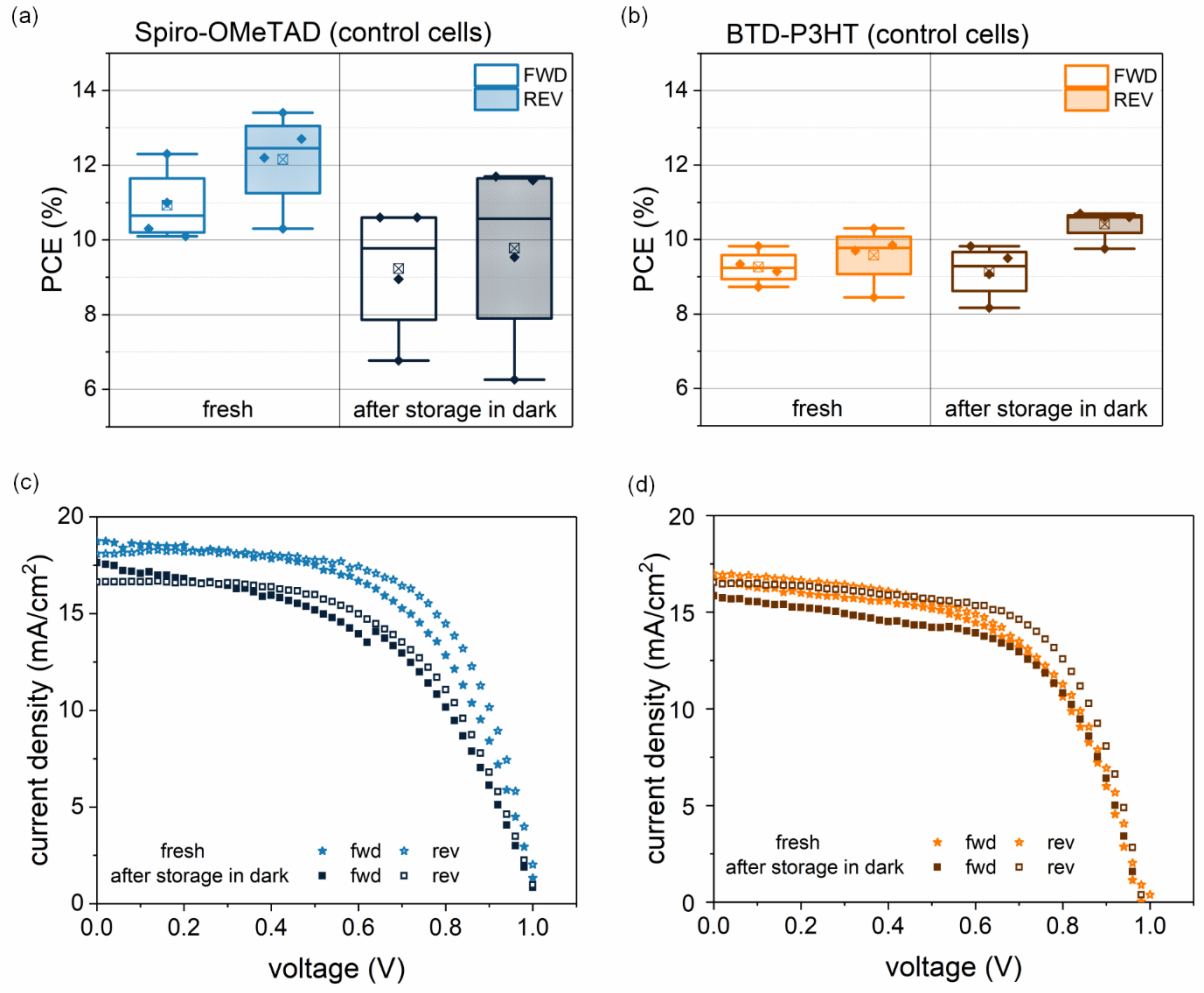

Figure 2. ***Effect of storage time on control cells.*** *Control cells were tested after fabrication and after being stored in a box, in the dark at ambient conditions, for as long as the time needed to ship the other cells to the ISIS facility, where they were irradiated, and then back to the fabrication laboratory. (a), (b) Power conversion efficiency for control cells endowed with spiro-OMeTAD and BTD-P3HT respectively; values for both forward scan (from short to open circuit, blank boxes) and reverse scan (from open to short circuit, patterned boxes) are reported. (c), (d) J-V curves of the same cells, representing an average of four devices.*

The electrical behaviour of the control cells after the storage in dark was compared to that of the irradiated devices to assess the effect of neutron irradiation. In Figure 3, average J-V curves are reported as well as the variation in the PV parameters (Figure S6) for the irradiated samples with respect to the relative controls.

The efficiency of spiro-OMeTAD cells, irradiated at 10^9 neutrons·cm^{-2} fluence, decreased by 7% in average in forward scan and increased by about 5% in average in reverse scan; at higher fluence, i.e. 10^{10} neutrons·cm^{-2}, the PCE dropped in average by 16% (forward) and

11% (reverse). The performance of irradiated BTD-P3HT cells also decreased, with more pronounced PCE drop and hysteresis for the 10^9 neutrons·cm^{-2} fluence, i.e. -31% and -18% for the forward and reverse scans respectively. Overall, BTD-P3HT cells degraded more than spiro-OMeTAD devices under 10^9 neutrons·cm^{-2} irradiation, and similarly to spiro-OMeTAD under 10^{10} neutrons·cm^{-2} irradiation (13-16% drop).

Still, open circuit voltage (V_{OC}) displayed a quite uniform 2.5% decrement for BTD-P3HT cells, regardless the fluence and the scan direction, whereas for spiro-OMeTAD it decreased by about 4% and 8% respectively with the increase of the irradiation fluence. Shorter charge carrier lifetime and thus higher recombination rate are very likely for all irradiated samples, but to a higher extent for spiro-OMeTAD. High energy neutrons are known to induce atomic displacement, resulting in the creation of vacancies and interstitial sites (Frenkel pairs)[28], and are also capable of ionizing the perovskite crystal lattice, damaging its crystal structure by upsetting the ionic and covalent bonds between atoms[25]. Both phenomena lead to energy states in the band gap near the valence or conduction band that act as recombination centres, lowering the V_{OC}.

Short circuit current density (J_{SC}) dropped by about 10% for all BTD-P3HT devices, with the exception of the 10^{10} neutrons·cm^{-2} irradiated samples (-4.5%, reverse). Spiro-OMeTAD cells experienced an even more severe loss, with larger difference between forward and reverse scan values: -8% in forward and -16% in reverse for 10^9 neutrons·cm^{-2}, -7% in forward and -22% in reverse for 10^{10} neutrons·cm^{-2}. The lower J_{SC} values point to a higher degree of degradation of the perovskite film for the spiro-OMeTAD cells than for the BTD-P3HT; the higher hysteresis can be ascribed to excess irradiation-induced vacancy and interstitial defects, causing ion and charge carrier migration in the active layer and altering the build-in potential[21,48,49].

For spiro-OMeTAD devices under both fluences, such J_{SC} values, lower than the controls, especially in reverse, caused positive variations for the fill factor (FF). Irradiated cells showed in average 75% FF for 10^9 neutrons·cm^{-2} fluence (+31% compared to control, reverse scan) and 73% FF for 10^{10} neutrons·cm^{-2} fluence (+28% compared to control, reverse scan); in forward scans, instead, FF values of irradiated cells (54% and 51% respectively) were comparable to the control. For all BTD-P3HT devices, FF variations were instead

negative, although below 6%, with the only exception of the 10^9 neutrons·cm^{-2} irradiated cells in reverse scan, which lost around 22% compared to the control and displayed a higher hysteresis degree than the 10^{10} neutrons·cm^{-2} irradiated ones.

The observed PCE reduction for both HTMs, due mainly to the J_{SC} drop, can be the result of degradation of the hole transport layer and of its interface with the perovskite layer, leading to shallow trap states, and has been reported for devices under neutron[28] and proton irradiation[21].

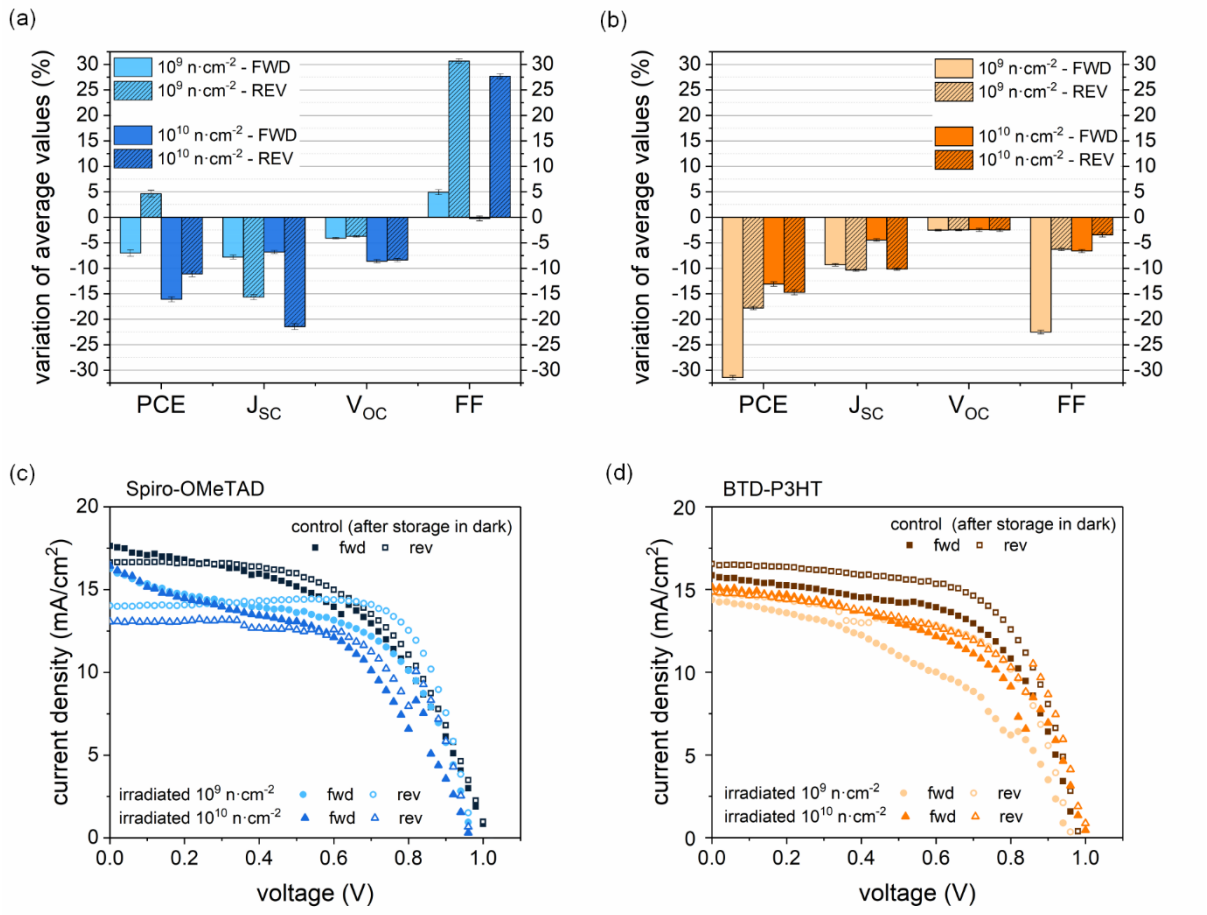

Figure 3. ***Effect of neutron irradiation on flexible cells.*** *(a), (b) Variation of the average values of PV parameters for the irradiated flexible cells, with either spiro-OMeTAD or BTD-P3HT as the HTL compared to control cells. (c), (d) J-V curves, representing an average of four devices, for the same flexible devices: control cells and cells irradiated at different fluences, i.e. 10^9 and 10^{10} neutrons·cm^{-2}·s^{-1}.*

External quantum efficiency (EQE) spectra confirm the performance trends: initial EQE is higher for spiro-OMeTAD control cells than for BTD-P3HT, as shown in Figure 4, leading to integrated photocurrent of 17.9 and 13.8 mA·cm^{-2}, respectively, in line with average J_{SC} values from J-V measurements. For irradiated samples, regardless the fluence, the spectra are almost identical, lower in intensity than the controls. Nevertheless, the drop in EQE, and thus in the integrated photocurrent density, is larger for spiro-OMeTAD than for BTD-P3HT cells after irradiation (around 20% and 10% lower than the control, respectively). Reduction of EQE intensity, can indicate a higher degree of degradation of the HTM and/or of the HTM/perovskite interface. The spectrum shape of irradiated spiro-OMeTAD cells resembles the controls, with a slight red shift at low wavelength; EQE spectra of irradiated BTD-P3HT devices are slightly tilted, with more accentuated drop at higher wavelengths. Lower values in the high wavelengths region can be ascribable to an increase of PbI_2, which does not absorb beyond ~540 nm, in the perovskite layer, with consequent detrimental effect on its ability of photogenerating current.

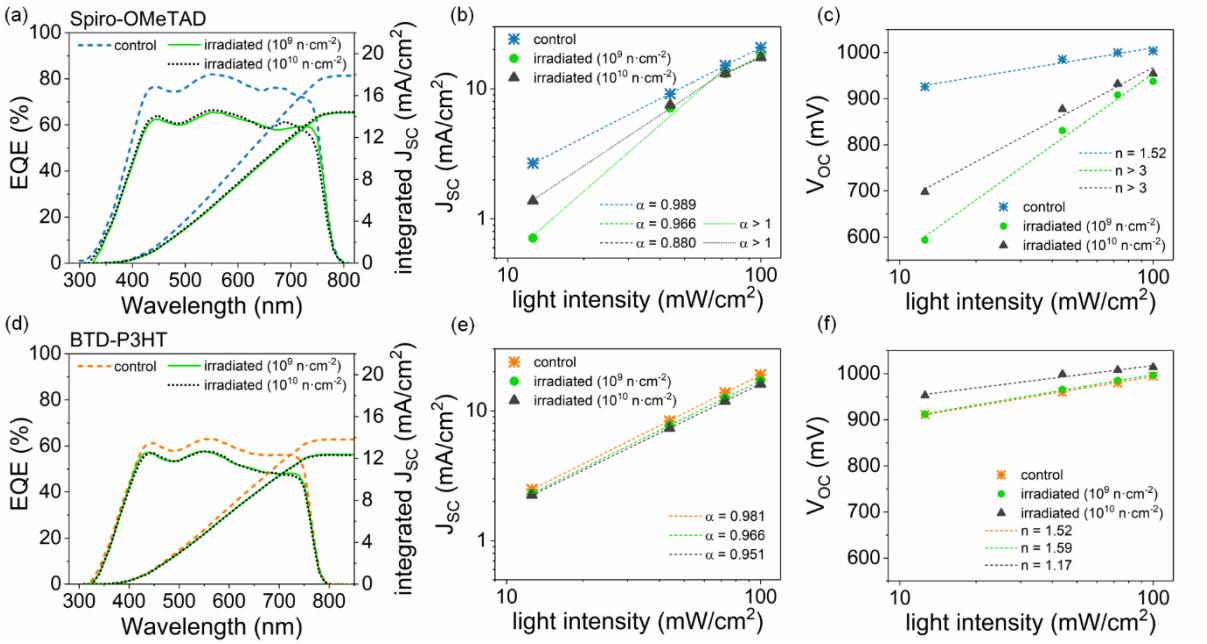

Figure 4. ***Characterisation of irradiated flexible cells.*** *(a, d) EQE spectra of the control and irradiated cells endowed with spiro-OMeTAD and BTD-P3HT respectively; (b, e) Short Circuit Current density and (c, f) Open Circuit Voltage as functions of light intensity for representative flexible cells using spiro-OMeTAD and BTD-P3HT as the hole transport material.*

Further insights on the effect of the neutron irradiation come from the exponent α and ideality factor n, extracted respectively from the double logarithmic J_{SC} and semilogarithmic V_{OC} trends with light intensity (Figure 4). When BTD-P3HT is used as the HTM, α is close to 1 for all samples, slightly lower for the irradiated cells (0.966 and 0.951 respectively) than the control, i.e. 0.981: space charge effects are negligible and charge transport is not compromised. For spiro-OMeTAD cells, instead, α is close to 1 for the control but, for the irradiated cells, it sharply increases, especially at low light intensities, denoting a possible increase of bimolecular recombination mechanisms [50]. A similar trend is observed for V_{OC} as a function of light intensity: BTD-P3HT cells display similar slope, thus similar values of the ideality factor for both control and 10^9 neutrons·cm^{-2} irradiated cell (i.e. 1.52 and 1.59 respectively) and even a lower value (i.e. 1.17) for 10^{10} neutrons·cm^{-2} irradiated cells, pointing to similar, even reduced, recombination rates for the irradiated samples to the control. On the other hand, the increasingly steeper slope with fluence for irradiated spiro-OMeTAD cells, compared to the control, denotes an increased trap-mediated recombination, confirming the detrimental effect of neutron-induced defects on V_{OC} and performance in general, as discussed above.

Conclusions

The performance of unencapsulated PSC devices on flexible substrates were assessed before and after neutron irradiation at two different fluences. Commercially available spiro-OMeTAD and in-house synthesized BTD-P3HT were compared.

BTD-P3HT showed limited V_{OC} and J_{SC} losses compared to spiro-OMeTAD but the overall performance suffered a much higher PCE drop, especially at lower fluence, resulting from a larger decrease in FF, very likely due to a not optimal perovskite/polymer interface, more prone to degradation.

Nonetheless, a smaller decrease in the spectral response characterized BTD-P3HT devices compared to spiro-OMeTAD ones as well as only slight changes in the behavior at different light intensities, suggesting the polymer can be potentially more resilient than spiro-OMeTAD under neutron irradiation, once the interfacial issues are addressed. Further

efforts and investigations are indeed needed to further optimize the modified polymer and also to gain more insights on the interaction between neutrons and perovskite PV, especially on flexible substrates, to speed up the adoption of such promising devices for space and avionic applications.

Acknowledgements

The authors would like to acknowledge the Italian Space Agency (ASI) for funding the PEROSKY project.

FDR, BT, FB would like to acknowledge the European Union's Horizon 2020 Research and Innovation Programme under grant agreement No763989 APOLO. This publication reflects only the author's views and the European Union is not liable for any use that may be made of the information contained therein.

NYN and ADC acknowledge the support of the Italian Ministry of Economic Development in the framework of the Operating Agreement with ENEA for Research on the Electric System.

Neutron beam time was provided by ChipIR (DOI: 10.5286/ISIS.E.RB2000137).

Contribution of the authors :

Francesca De Rossi: Conceptualization, Methodology, Investigation, Formal analysis, Visualization, Validation, Writing – Original Draft, Writing – Review & Editing.

Babak Taheri: Investigation, Methodology, Formal analysis, Visualization, Validation, Writing – Original Draft, Writing – Review & Editing.

Matteo Bonomo: Conceptualization, Validation, Formal analysis, Investigation, Data Curation, Writing - Original Draft, Writing - Review & Editing, Visualization.

Vishal Gupta: Conceptualization, Validation, Formal analysis, Resources, Writing - Original Draft.

Giacomo Renno: Validation, Data Curation, Visualization.

Narges Yaghoobi Nia: Investigation, Validation, Writing - Review & Editing.

Paolo Rech: Conceptualization, Investigation, Resources, Writing - Review & Editing, Supervision, Project administration, Funding acquisition.

Chris Frost: Investigation, Resources, Project administration.

Carlo Cazzaniga: Investigation, Resources, Writing - Review & Editing.

Pierluigi Quagliotto: Validation; Formal analysis; Resources; Data Curation; Writing - Review & Editing; Supervision.

Aldo Di Carlo: Writing - Review & Editing; Supervision; Project administration; Funding acquisition.

Claudia Barolo: Conceptualization; Writing - Review & Editing; Supervision; Project administration; Funding acquisition.

Marco Ottavi: Conceptualization, Validation, Formal analysis, Resources, Writing - Review & Editing, Supervision, Project administration.

Francesca Brunetti: Conceptualization; Validation; Formal analysis; Writing - Review & Editing; Supervision; Resources; Project administration; Funding acquisition.

SUPPORTING INFORMATION

Experimental

Fabrication of devices

ITO PET substrates (15 Ω/sq), sized 2.5 x 2.5 cm^2 and laser scribed to obtain 4 electrically isolated areas on the same substrate, were cleaned by ultrasonication with isopropanol and water for 15 minutes in each solvent. The electron transport layer SnO_2 was obtained via spin coating of a SnO_2 nanoparticle aqueous dispersion (15%w, Alfa Aesar) at a speed of 6000 rpm for 35 seconds. After annealing at 100 °C for 1 hour, substrates were brought into a N2 filled glove box for the perovskite layer deposition.

The perovskite precursor solution was prepared mixing 166 mg FAI, 21.6 mg MABr, 87.1 mg $PbBr_2$, 547.4 mg PbI_2 and 19.4 mg of CsI and adding N-N dimethylformamide (DMF) and dimethyl sulfoxide (DMSO) at volume ratio of 3.16 and then leaving it to stir for 12 hours at room temperature. The spin coating deposition of the perovskite was performed at 1000 rpm for 10 s followed by a high-speed step at 5000 rpm for 30 seconds. During this last step,

150 µL of CB was dripped as anti-solvent onto the spinning substrate. The samples were annealed at 100 °C for 1 hour.

Spiro-OMeTAD (2,2',7,7'-Tetrakis[N,N-di(4-methoxyphenyl)amino]-9,9'-spirobifluorene) was used as the reference hole transport layer: 16.6 µl of bis(trifluoromethylsulfonyl)imide lithium salt in acetonitrile (Li-TFSI, 520 mg/ml), 7.2 µl of cobalt (III) tris(bis(trifluoromethylsulfonyl)imide) (FK-209, 0.25 M in acetonitrile), 27 µL of 4 tert-butylpyridine (TBP) were added to 73.5 mg of spiro-OMeTAD dissolved in 1 ml of chlorobenzene. The solution was spun at 2000 rpm for 20 seconds.

A benzothiadiazole-modified poly(3-hexylthiophene-2,5-diyl), i.e. BTD-P3HT, in-house synthesised, was also tested as HTM: it was dissolved with a concentration of 12 mg/ml in chlorobenzene and then doped by adding Li-TFSI, TBP, and Co(III)-TFSI, following doping strategy procedure previously reported[36]. To prevent any agglomeration, solution was kept stirring at 50 °C for 15 min, then deposited by spin-coating at 6000 rpm for 45 seconds.

The devices were finished by thermally evaporating 90 nm of gold as the top electrode.

Synthesis of BTD-P3HT

The synthesis (a Kumada polycondensation reaction) of the in-house HTM is detailly described in our precedent paper[29] and it is just briefly recalled hereafter: in a Schlenk flask, 4,7-bis(5-bromo-3-hexylthiophen-2-yl)benzo[c][1,2,5]thiadiazole (0.4 g, 0.63 mmol) was mixed with lithium chloride (0.5 M in THF, 1.40 mL, 0.7 mmol) and iPrMgCl (2 M in THF, 0.35 mL, 0.7 mmol) in dry THF (1.5 mL) under Argon atmosphere. The mixture was stirred at room temperature for 2 hours. Similarly,2-bromo-3-hexyl-5-iodothiophene (4.5 g, 12.1 mmol) was mixed with lithium chloride (0.5 M in THF, 26.5 mL, 13.3 mmol), dry THF (65 mL) and iPrMgCl (2 M in THF, 6 mL, 12.1 mmol). The mixture was stirred at room temperature for 1hour. The two solutions obtained were mixed together into a Schlenk flask. Then 0.5% mol of Ni(iPr)$(acac)_2$, as catalyst, in dry THF solution (10 mmol/L, 6.35 mL) was added and the mixture was thoroughly stirred for 30 minutes at room temperature. The polymerization was quenched by adding few drops of aqueous HCl (5 mol/L). The mixture was poured into petroleum ether and stirred for 45 min to precipitate the polymer that was then washedwith water and acetone. The product was collected by filtration and then dried in

vacuum (800 mbar, 25°C). Yield: 13.55%. ^{1}H-NMR (128 scan, 50 °C, 600 MHz, $CDCl_3$, ppm) δ:6.98 (s, 1H), 2.81 (t, J = 7.9 Hz, 2H), 1.72 (t, J = 7.7 Hz, 2H), 1.40 – 1.26 (m, 6H), 0.92 (t, J = 7.3, 5.5, 2.8 Hz, 3H).

Characterisation of films and devices

UV-Vis spectra were measured by using a spectrophotometer (Dymax EC-5000 lamp) in a wavelength range of 300–850 nm.

Current density-voltage (J-V) curves were recorded under illumination by a solar simulator (ABET Sun 2000), set at AM 1.5 and calibrated to 100 mW·cm^2 using a calibrated silicon reference cell. The 4 cells on each 2.5x2.5 cm^2 substrates were measured at the same time, in both forward and reverse direction, with a scan rate of 100 mV·s, by a commercial setup of 4-wire source meter and several channels (Arkeo-Ariadne, Cicci Research srl). The active areas were delimited by using black tape masks with apertures of 0.09 cm^2.

EQE spectra were measured using a commercial setup (Arkeo-Ariadne, Cicci Research srl) based on a 300 W xenon lamp, able to acquire a spectrum from 300 to 1100 nm with a resolution of 2 nm. The same setup, endowed with white LEDs (4100 Kelvin) and a 4-wire source meter, allowed measuring J-V plots at increasing light intensities.

The powder X-ray diffraction patterns (VTXRD) were collected with an X'Pert PRO MPD diffractometer from PANalytical working in Bragg–Brentano geometry equipped with a Cu K_α source. Scattered photons were revealed by an X'celerator linear detector equipped with a Ni filter to attenuate K_β.

Additional Figures

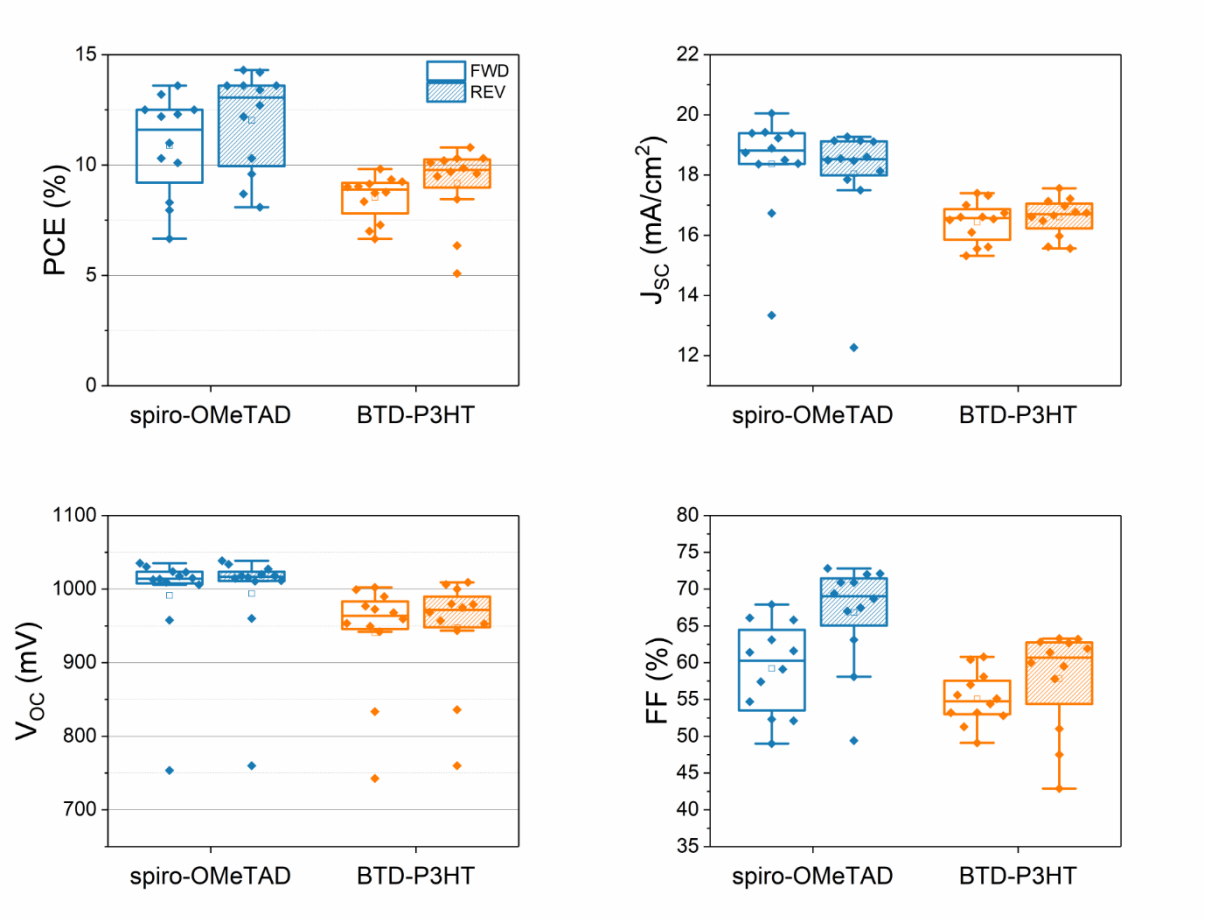

Figure S 1. Photovoltaic parameters of flexible cells endowed with BTD-P3HT and spiro-OMeTAD as hole transport materials after fabrication, before being shipped for neutron irradiation. Values for both forward (from short to open circuit, blank boxes) and reverse (from open to short circuit, patterned boxes) are reported.

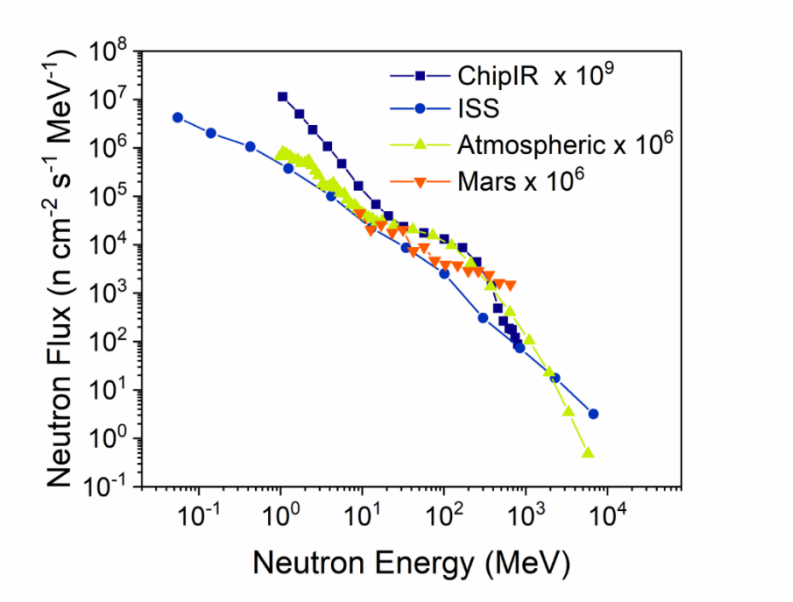

Figure S 2. ***Neutrons energy spectra.*** *Energy spectrum using the ChipIR beamline compared to energy spectra on the ISS, terrestrial atmosphere and Mars, respectively.*

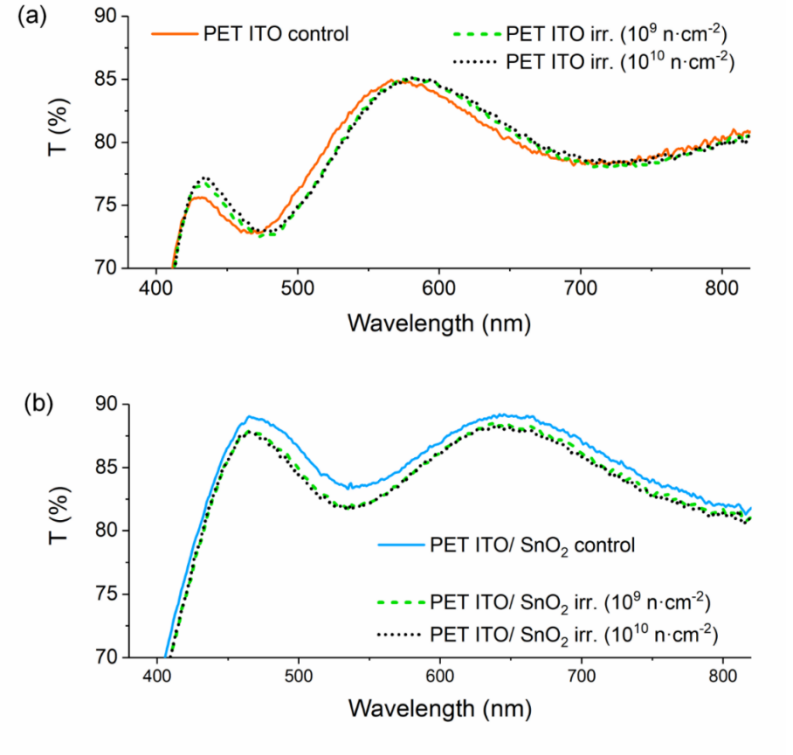

Figure S 3. Transmittance of bare PET ITO substrates and SnO_2 films on PET ITO showing no significance variation between control and irradiated samples.

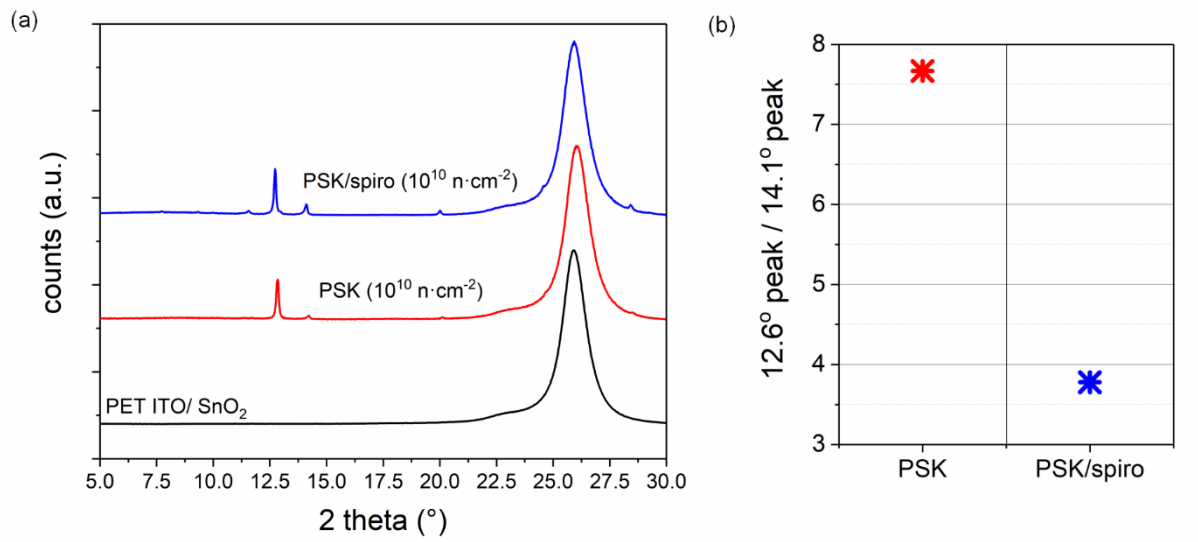

Figure S 4. (a) XRD spectra of perovskite and perovskite/spiro-OMeTAD films after the irradiation at 10^{10} neutrons·cm^{-2}; (b) ratio between the PbI_2 peak at 12.6° and the perovskite peak at 14.1° for the same films: higher values of this ratio are associated to larger degradation of the perovskite layer.

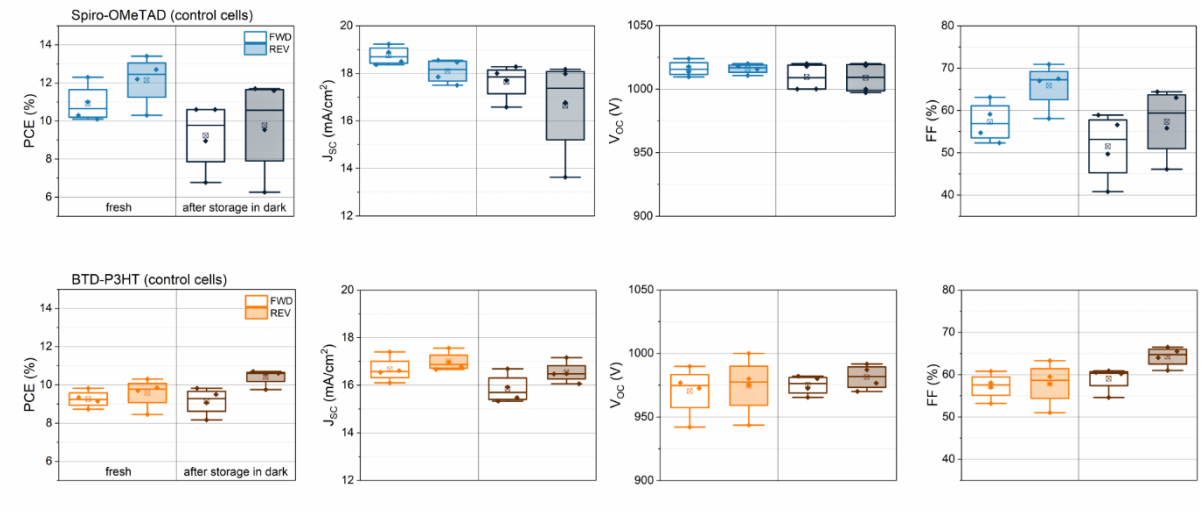

Figure S 5. Effect of storage time on control cells: cells were tested after fabrication and after being stored in a box, in air and in the dark at ambient conditions, for as long as the time needed to ship the other cells to the ISIS where they were irradiated and then shipped back. Values for both forward (from short to open circuit, blank boxes) and reverse (from open to short circuit, patterned boxes) are reported.

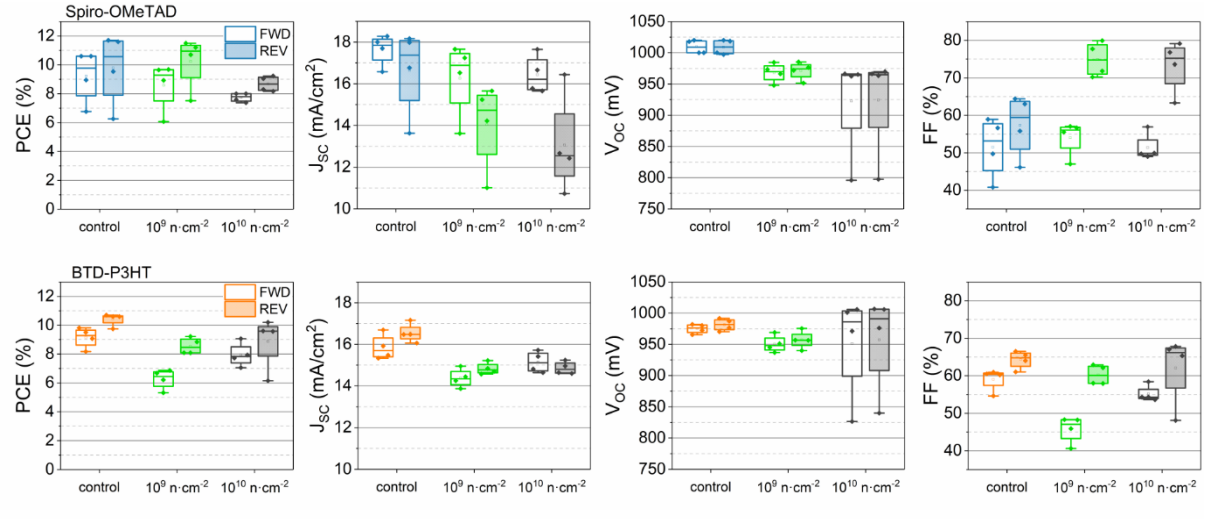

Figure S 6. ***Effect of neutron irradiation on flexible cells.*** *PV parameters for spiro-OMeTAD(top) and BTD-P3HT (bottom) flexible cells after irradiation at different fluences, i.e.10^9 and 10^{10} neutrons·cm^{-2}·s^{-1}, compared to control cells, after storage in dark for 21 days. Values for both forward (from short to open circuit, blank boxes) and reverse (from open to short circuit, patterned boxes) are reported.*

[1] H. Pan, X. Zhao, G. Xiu, H. Li, N. Ladi, X. Zhang, W. Huang, S. Ahmad, L. Ding, Y. Shen, M. Wang, Y.Q. Fu, Advances in design engineering and merits of electron transporting layers in perovskite solar cells, Mater. Horizons. (2020). https://doi.org/10.1039/d0mh00586j.

[2] M. Jung, S.-G.G. Ji, G. Kim, S. Il Seok, Perovskite precursor solution chemistry: From fundamentals to photovoltaic applications, Chem. Soc. Rev. 48 (2019) 2011–2038. https://doi.org/10.1039/c8cs00656c.

[3] M. Duan, Y. Hu, A. Mei, Y. Rong, H. Han, Printable carbon-based hole-conductor-free mesoscopic perovskite solar cells: From lab to market, Mater. Today Energy. 7 (2018) 221–231. https://doi.org/10.1016/j.mtener.2017.09.016.

[4] N.G. Park, K. Zhu, Scalable fabrication and coating methods for perovskite solar cells and solar modules, Nat. Rev. Mater. 5 (2020) 333–350. https://doi.org/10.1038/s41578-019-0176-2.

[5] F. Lang, O. Shargaieva, V. V. Brus, H.C. Neitzert, J. Rappich, N.H. Nickel, Influence of Radiation on the Properties and the Stability of Hybrid Perovskites, Adv. Mater. 30 (2018) 1702905. https://doi.org/10.1002/adma.201702905.

[6] K. Domanski, E.A. Alharbi, A. Hagfeldt, M. Grätzel, W. Tress, Systematic investigation of the impact of operation conditions on the degradation behaviour of perovskite solar cells, Nat. Energy. 3 (2018) 61–67. https://doi.org/10.1038/s41560-017-0060-5.

[7] M. V. Khenkin, E.A. Katz, A. Abate, G. Bardizza, J.J. Berry, C. Brabec, F. Brunetti, V. Bulović, Q. Burlingame, A. Di Carlo, R. Cheacharoen, Y.-B. Cheng, A. Colsmann, S. Cros, K. Domanski, M. Dusza, C.J. Fell, S.R. Forrest, Y. Galagan, D. Di Girolamo, M. Grätzel, A. Hagfeldt, E. von Hauff, H. Hoppe, J. Kettle, H. Köbler, M.S. Leite, S. Liu, Y.-L. Loo, J.M. Luther, C.-Q. Ma, M. Madsen,

M. Manceau, M. Matheron, M. McGehee, R. Meitzner, M.K. Nazeeruddin, A.F. Nogueira, Ç. Odabaşı, A. Osherov, N.-G. Park, M.O. Reese, F. De Rossi, M. Saliba, U.S. Schubert, H.J. Snaith, S.D. Stranks, W. Tress, P.A. Troshin, V. Turkovic, S. Veenstra, I. Visoly-Fisher, A. Walsh, T. Watson, H. Xie, R. Yıldırım, S.M. Zakeeruddin, K. Zhu, M. Lira-Cantu, Consensus statement for stability assessment and reporting for perovskite photovoltaics based on ISOS procedures, Nat. Energy. 5 (2020) 35–49. https://doi.org/10.1038/s41560-019-0529-5.

[8] Y. Zhao, Q. Ye, Z. Chu, F. Gao, X. Zhang, J. You, Recent Progress in High-efficiency Planar-structure Perovskite Solar Cells, ENERGY Environ. Mater. 2 (2019) 93–106. https://doi.org/10.1002/eem2.12042.

[9] G. Schileo, G. Grancini, Halide perovskites: current issues and new strategies to push material and device stability, J. Phys. Energy. 2 (2020) 021005. https://doi.org/10.1088/2515-7655/ab6cc4.

[10] NREL, Best Research-Cell Efficiency Chart | Photovoltaic Research | NREL, Best Res. Effic. Chart | Photovolt. Res. | NREL. (2021) https://www.nrel.gov/pv/cell-efficiency.html. https://www.nrel.gov/pv/cell-efficiency.html (accessed April 28, 2021).

[11] K. Huang, Y. Peng, Y.Y. Gao, J. Shi, H. Li, X. Mo, H. Huang, Y.Y. Gao, L. Ding, J. Yang, High-Performance Flexible Perovskite Solar Cells via Precise Control of Electron Transport Layer, Adv. Energy Mater. 9 (2019) 1901419. https://doi.org/10.1002/aenm.201901419.

[12] P. Zeng, W. Deng, M. Liu, Recent Advances of Device Components toward Efficient Flexible Perovskite Solar Cells, Sol. RRL. 4 (2020) 1900485. https://doi.org/10.1002/solr.201900485.

[13] J. Zhang, W. Zhang, H.M. Cheng, S.R.P. Silva, Critical review of recent progress of flexible perovskite solar cells, Mater. Today. (2020). https://doi.org/10.1016/j.mattod.2020.05.002.

[14] J. Dagar, S. Castro-Hermosa, M. Gasbarri, A.L. Palma, L. Cina, F. Matteocci, E. Calabrò, A. Di Carlo, T.M. Brown, Efficient fully laser-patterned flexible perovskite modules and solar cells based on low-temperature solution-processed SnO 2 /mesoporous-TiO 2 electron transport layers, Nano Res. 11 (2018) 2669–2681. https://doi.org/10.1007/s12274-017-1896-5.

[15] D. Yang, R. Yang, S. Priya, S. (Frank) Liu, Recent Advances in Flexible Perovskite Solar Cells: Fabrication and Applications, Angew. Chemie - Int. Ed. 58 (2019) 4466–4483. https://doi.org/10.1002/anie.201809781.

[16] M. Davis, Z. Yu, A review of flexible halide perovskite solar cells towards scalable manufacturing and environmental sustainability, J. Semicond. 41 (2020) 41603. https://doi.org/10.1088/1674-4926/41/4/041603.

[17] J. Long, Z. Huang, J. Zhang, X. Hu, L. Tan, Y. Chen, Flexible perovskite solar cells: Device design and perspective, Flex. Print. Electron. 5 (2020) 013002. https://doi.org/10.1088/2058-8585/ab556e.

[18] H.S. Jung, G.S. Han, N.G. Park, M.J. Ko, Flexible Perovskite Solar Cells, Joule. 3 (2019) 1850–1880. https://doi.org/10.1016/j.joule.2019.07.023.

[19] N. Mariotti, M. Bonomo, C. Barolo, Emerging Photovoltaic Technologies and Eco-Design—Criticisms and Potential Improvements, in: Reliab. Ecol. Asp. Photovolt. Modul., IntechOpen, 2020. https://doi.org/10.5772/intechopen.88327.

[20] M. Kaltenbrunner, G. Adam, E.D. Głowacki, M. Drack, R. Schwödiauer, L. Leonat, D.H. Apaydin, H. Groiss, M.C. Scharber, M.S. White, N.S. Sariciftci, S. Bauer, Flexible high power-per-weight perovskite solar cells with chromium oxide-metal contacts for improved stability

in air, Nat. Mater. 14 (2015) 1032–1039. https://doi.org/10.1038/nmat4388.

[21] J. Barbé, D. Hughes, Z. Wei, A. Pockett, H.K.H. Lee, K.C. Heasman, M.J. Carnie, T.M. Watson, W.C. Tsoi, Radiation Hardness of Perovskite Solar Cells Based on Aluminum-Doped Zinc Oxide Electrode Under Proton Irradiation, Sol. RRL. 3 (2019) 1900219. https://doi.org/10.1002/solr.201900219.

[22] Y. Miyazawa, M. Ikegami, H.W. Chen, T. Ohshima, M. Imaizumi, K. Hirose, T. Miyasaka, Tolerance of Perovskite Solar Cell to High-Energy Particle Irradiations in Space Environment, IScience. 2 (2018) 148–155. https://doi.org/10.1016/j.isci.2018.03.020.

[23] F. Lang, N.H. Nickel, J. Bundesmann, S. Seidel, A. Denker, S. Albrecht, V. V. Brus, J. Rappich, B. Rech, G. Landi, H.C. Neitzert, Radiation Hardness and Self-Healing of Perovskite Solar Cells, Adv. Mater. 28 (2016) 8726–8731. https://doi.org/10.1002/adma.201603326.

[24] V. V. Brus, F. Lang, J. Bundesmann, S. Seidel, A. Denker, B. Rech, G. Landi, H.C. Neitzert, J. Rappich, N.H. Nickel, Defect Dynamics in Proton Irradiated CH3NH3PbI3 Perovskite Solar Cells, Adv. Electron. Mater. 3 (2017). https://doi.org/10.1002/aelm.201600438.

[25] O. Malinkiewicz, M. Imaizumi, S.B. Sapkota, T. Ohshima, S. Öz, Radiation effects on the performance of flexible perovskite solar cells for space applications, Emergent Mater. 3 (2020) 9–14. https://doi.org/10.1007/s42247-020-00071-8.

[26] T.W. Armstrong, B.L. Colborn, Predictions of secondary neutrons and their importance to radiation effects inside the international space station, Radiat. Meas. 33 (2001) 229–234. https://doi.org/10.1016/S1350-4487(00)00152-9.

[27] C. Constantinescu, Trends and challenges in VLSI circuit reliability, IEEE Micro. 23 (2003) 14–19. https://doi.org/10.1109/MM.2003.1225959.

[28] G.M. Paternò, V. Robbiano, L. Santarelli, A. Zampetti, C. Cazzaniga, V. Garcìa Sakai, F. Cacialli, Perovskite solar cell resilience to fast neutrons, Sustain. Energy Fuels. 3 (2019) 2561–2566. https://doi.org/10.1039/c9se00102f.

[29] F. De Rossi, G. Renno, B. Taheri, N. Yaghoobi Nia, V. Ilieva, A. Fin, A. Di Carlo, M. Bonomo, C. Barolo, F. Brunetti, Modified P3HT materials as hole transport layers for flexible perovskite solar cells, J. Power Sources. 494 (2021) 229735. https://doi.org/10.1016/j.jpowsour.2021.229735.

[30] R.S. Sanchez, E. Mas-Marza, Light-induced effects on Spiro-OMeTAD films and hybrid lead halide perovskite solar cells, Sol. Energy Mater. Sol. Cells. 158 (2016) 189–194. https://doi.org/10.1016/j.solmat.2016.03.024.

[31] A.K. Jena, M. Ikegami, T. Miyasaka, Severe Morphological Deformation of Spiro-OMeTAD in (CH3NH3)PbI3 Solar Cells at High Temperature, ACS Energy Lett. 2 (2017) 1760–1761. https://doi.org/10.1021/acsenergylett.7b00582.

[32] G. Kim, H. Min, K.S. Lee, D.Y. Lee, S.M. Yoon, S. Il Seok, Impact of strain relaxation on performance of a-formamidinium lead iodide perovskite solar cells, Science (80-.). 370 (2020) 108–112. https://doi.org/10.1126/science.abc4417.

[33] M. Jeong, I.W. Choi, E.M. Go, Y. Cho, M. Kim, B. Lee, S. Jeong, Y. Jo, H.W. Choi, J. Lee, J.H. Bae, S.K. Kwak, D.S. Kim, C. Yang, Stable perovskite solar cells with efficiency exceeding 24.8% and 0.3-V voltage loss, Science (80-.). 369 (2020) 1615–1620. https://doi.org/10.1126/science.abb7167.

[34] M. Zhang, M. Lyu, H. Yu, J.H. Yun, Q. Wang, L. Wang, Stable and low-cost mesoscopic CH3NH3PbI2Br perovskite solar cells by using a thin poly(3-hexylthiophene) layer as a hole transporter, Chem. - A Eur. J. 21 (2015) 434–439. https://doi.org/10.1002/chem.201404427.

[35] Y. Yang, Y. Liu, Z. Hong, Q. Chen, H. Chen, W.H. Chang, T. Bin Song, Perovskite Solar Cells Employing Dopant-Free Organic Hole Transport Materials with Tunable Energy Levels, Adv. Mater. 28 (2016) 440–446. https://doi.org/10.1002/adma.201504293.

[36] N. Yaghoobi Nia, E. Lamanna, M. Zendehdel, A.L. Palma, F. Zurlo, L.A. Castriotta, A. Di Carlo, Doping Strategy for Efficient and Stable Triple Cation Hybrid Perovskite Solar Cells and Module Based on Poly(3-hexylthiophene) Hole Transport Layer, Small. 15 (2019) 1904399. https://doi.org/10.1002/smll.201904399.

[37] N. Yaghoobi Nia, M. Bonomo, M. Zendehdel, E. Lamanna, M. Desoky, H., B. Paci, F. Zurlo, A. Generosi, C. Barolo, G. Viscardi, P. Quagliotto, A. Di Carlo, The Impact of P3HT Regioregularity and Molecular Weight on the Efficiency and Stability of Perovskite Solar Cells, Under Rev. (2021).

[38] J.W. Jung, J.S. Park, I.K. Han, Y. Lee, C. Park, W. Kwon, M. Park, Flexible and highly efficient perovskite solar cells with a large active area incorporating cobalt-doped poly(3-hexylthiophene) for enhanced open-circuit voltage, J. Mater. Chem. A. 5 (2017) 12158–12167. https://doi.org/10.1039/c7ta03541a.

[39] J.C. Brauer, Y.H. Lee, M.K. Nazeeruddin, N. Banerji, Charge Transfer Dynamics from Organometal Halide Perovskite to Polymeric Hole Transport Materials in Hybrid Solar Cells, J. Phys. Chem. Lett. 6 (2015) 3675–3681. https://doi.org/10.1021/acs.jpclett.5b01698.

[40] N.Y. Nia, F. Matteocci, L. Cina, A. Di Carlo, High-Efficiency Perovskite Solar Cell Based on Poly(3-Hexylthiophene): Influence of Molecular Weight and Mesoscopic Scaffold Layer, ChemSusChem. 10 (2017) 3854–3860. https://doi.org/10.1002/cssc.201700635.

[41] N. Wu, Y. Wu, D. Walter, H. Shen, T. Duong, D. Grant, C. Barugkin, X. Fu, J. Peng, T. White, K. Catchpole, K. Weber, Identifying the Cause of Voltage and Fill Factor Losses in Perovskite Solar Cells by Using Luminescence Measurements, Energy Technol. 5 (2017) 1827–1835. https://doi.org/10.1002/ente.201700374.

[42] C. Cazzaniga, C.D. Frost, Progress of the Scientific Commissioning of a fast neutron beamline for Chip Irradiation, in: J. Phys. Conf. Ser., Institute of Physics Publishing, 2018: p. 012037. https://doi.org/10.1088/1742-6596/1021/1/012037.

[43] S. Feng, C. Cazzaniga, T. Minniti, M. Nocente, C. Frost, G. Gorini, A. Muraro, S. Romano, M. Tardocchi, Response of a telescope proton recoil spectrometer based on a YAP: Ce scintillator to 5–80 MeV protons for applications to measurements of the fast neutron spectrum at the ChipIr irradiation facility, Nucl. Instruments Methods Phys. Res. Sect. A Accel. Spectrometers, Detect. Assoc. Equip. 912 (2018) 36–38. https://doi.org/10.1016/j.nima.2017.10.026.

[44] J. Čermák, L. Mihai, D. Sporea, Y. Galagan, J. Fait, A. Artemenko, P. Štenclová, B. Rezek, M. Straticiuc, I. Burducea, Proton irradiation induced changes in glass and polyethylene terephthalate substrates for photovoltaic solar cells, Sol. Energy Mater. Sol. Cells. 186 (2018) 284–290. https://doi.org/10.1016/j.solmat.2018.06.046.

[45] Y. Rong, L. Liu, A. Mei, X. Li, H. Han, Beyond efficiency: The challenge of stability in mesoscopic perovskite solar cells, Adv. Energy Mater. 5 (2015). https://doi.org/10.1002/aenm.201501066.

[46] E.H. Jung, N.J. Jeon, E.Y. Park, C.S. Moon, T.J. Shin, T.Y. Yang, J.H. Noh, J. Seo, Efficient, stable and scalable perovskite solar cells using poly(3-hexylthiophene), Nature. 567 (2019) 511–515. https://doi.org/10.1038/s41586-019-1036-3.

[47] Z. Zhang, L. Qu, G. Shi, Fabrication of highly hydrophobic surfaces of conductive polythiophene, J. Mater. Chem. 13 (2003) 2858–2860. https://doi.org/10.1039/b309291g.

[48] V. Gupta, G. Lucarelli, S. Castro-Hermosa, T. Brown, M. Ottavi, Investigation of hysteresis in hole transport layer free metal halide perovskites cells under dark conditions, Nanotechnology. 31 (2020) 14. https://doi.org/10.1088/1361-6528/aba713.

[49] H.J. Snaith, A. Abate, J.M. Ball, G.E. Eperon, T. Leijtens, N.K. Noel, S.D. Stranks, J.T.W. Wang, K. Wojciechowski, W. Zhang, Anomalous hysteresis in perovskite solar cells, J. Phys. Chem. Lett. 5 (2014) 1511–1515. https://doi.org/10.1021/jz500113x.

[50] D. Yang, R. Yang, K. Wang, C. Wu, X. Zhu, J. Feng, X. Ren, G. Fang, S. Priya, S. (Frank) Liu, High efficiency planar-type perovskite solar cells with negligible hysteresis using EDTA-complexed SnO 2, Nat. Commun. 9 (2018) 3239. https://doi.org/10.1038/s41467-018-05760-x.

Declaration of interests

☒ The authors declare that they have no known competing financial interests or personal relationships that could have appeared to influence the work reported in this paper.

☐The authors declare the following financial interests/personal relationships which may be considered as potential competing interests: